Soft Matter

Accepted Manuscript

ROYAL SOCIETY OF CHEMISTRY

www.rsc.org/softmatter

Soft Matter

RSC Publishing

ARTICLE

Understanding the self-assembly of Fmoc-phenylalanine to hydrogel formation†

Cite this: DOI: 10.1039/x0xx00000x

Virender Singh[‡a], Kirti Snigdha[‡b], Chandan Singh[c], Neeraj Sinha[d], Ashwani Kumar Thakur*[a]

Received 00th April 2015,
Accepted 00th April 2015

DOI: 10.1039/x0xx00000x

www.rsc.org/

Hydrogels of low molecular weight molecules are important in biomedical applications. Multiple factors are responsible for hydrogel formation but, their role in governing self-assembly to hydrogel formation is poorly understood. Here we report the hydrogel formation of fluorenylmethyloxycarbonyl phenylalanine (FmocF) molecule. We used physical and thermal stimuli for solubilizing FmocF above the critical concentration to induce gel formation. The key role of Fmoc, Fmoc and phenylalanine covalent linkage, flexibility of phe side chain, pH, and buffer ions in self-assembly of FmocF to gel formation is described. We found that the collective action of different non-covalent interactions play role in making FmocF hydrogel. By using powder diffraction and infrared spectroscopy, we also report a new polymorphic form of FmocF after transitioning to hydrogel. In addition, we are proposing a model for drug release from FmocF hydrogel.

Introduction

Self-assembly refers to the process of spontaneous assembly of molecules into higher order structures due to intramolecular and intermolecular interactions.[1-3] Proteins, deoxyribonucleic acids (DNA) and lipids self-assemble into hierarchical structures to carry out different biological functions. Depending on the chemical nature of molecules, self-assembly can be driven by hydrogen bonding, electrostatic, van der Waals and π-π stacking interactions.[1-5] The phenomena of self-assembly is utilized in building versatile materials, biological mimics, and micro electronic items.[6] The work done on self-assembly of diphenylanaine[7,8], triphenylalanine[9], IKVAV, EAK-16[10] and other peptide amphiphiles[11,12] showed that they form varied micro and nano structures.[13] Off all these structures, hydrogels are commonly discussed due to their wide application ranging from tissue engineering, controlled drug delivery to nanoscale electronics.[6,14] One type of hydrogel is made up of amino acids, their derivatives and peptides. Peptide based hydrogelators self-assemble into polymer-like fibres using the non-covalent interactions and entraps large quantity of water molecules to form hydrogel.[15-17]

Apart from peptides, fluorenylmethyloxycarbonyl (Fmoc) protected amino acids have also been very effective hydrogelators.[18-21] These hydrogels have comparable physical and mechanical properties to those formed from longer peptides and covalently cross-linked polymers.[18,22-24] For the first time, the formation of hydrogels from Fmoc-protected dipeptides, Fmoc-Leu-Asp was described.[25] Then, Gazit *et al.* reported rapid self-assembly of Fmoc protected diphenylalanine into fibres with an average diameter of 10–100 nm that formed transparent hydrogel at physiological pH.[24,26] Hydrogels for growth of human dermal fibroblasts have also been developed by self-assembly of mixtures of FmocFF and Fmoc-RGD molecules.[27] Apart from Fmoc-diphenylalanine[28], Fmoc amino acid derivatives such as Fmoc-Phe, Fmoc-DOPA and Fmoc-Tyr are reported to form hydrogels.[29-31] Fluorescence, circular dichorism, FTIR, rheological property, have indicated an anti-parallel stacking of Fmoc groups through π-π stacking interactions to form β-sheet rich cylindrical fibrils that are entangled in hydrogels.[26,28] These studies efficiently predicted and devised a path to understand the mechanism of gel formation in Fmoc-modified dipeptide systems. This also shows the importance of elucidating the steps involved in hydrogelation process of Fmoc amino acids as their mechanism of hydrogelation is not yet known. Previously, we have reported the self-assembly mechanism of phenylalanine (Phe) into fibre formation and its modulation by D-Phe into flakes in relevance to phenylketonuria disease.[32] The self-assembly to fibre formation was found to be governed by mainly hydrophobic interactions.[32] Here we report the mechanistic details of gel formation by FmocF and main players involved in its formation. We have used physiological relevant buffer for hydrogel formation keeping in mind its potential use in biomedical applications. Using a range of spectroscopic methods, we gained an insight into the assembly process and transformation of FmocF solution to hydrogel. We report the specificity of gel formation by Phe with Fmoc. We also show a

new polymorphic form of FmocF in the gel state. Finally, we evaluated the dye release kinetics from this hydrogel.

Results and discussion

FmocF hydrogel formation

Hydrogel formation depends on the participating molecules, solvent type, pH of solvent, temperature and other variables. Phenylalanine is a hydrophobic amino acid and addition of Fmoc group further enhances the hydrophobicity of it, resulting in low water solubility. For hydrogel formation, super saturated solution of a molecule is required.[33] We have used FmocF as model molecule for hydrogel formation which consists of Fluorenylmethyloxycarbonyl (Fmoc) covalently linked to L-phenylalanine (Fig. 1a).

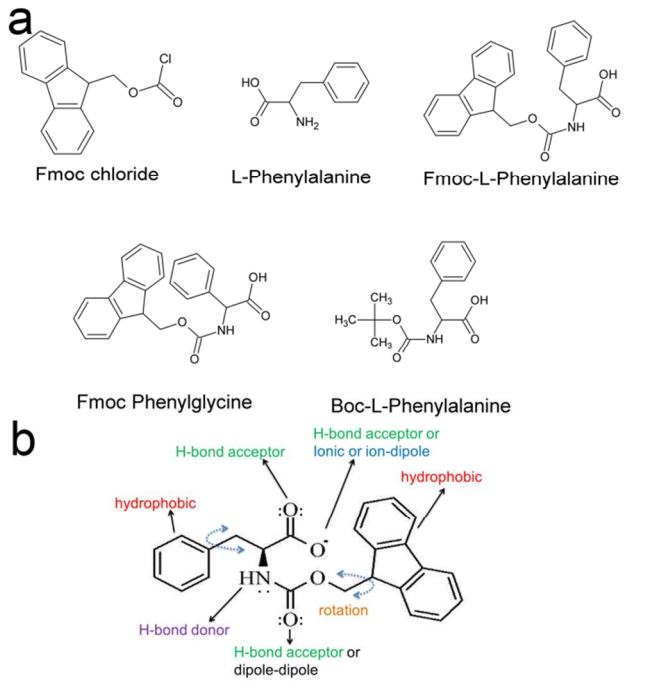

Fig. 1 (a) The chemical structural formulae of Fmoc chloride, L-phenylalanine, Fmoc-L-phenylalanine, Fmoc-phenylglycine and Boc-L-phenylalanine§. (b) FmocF structure highlighting potential sites of interactions.

To enhance the solubility of FmocF in water, sonication and heating procedures were employed to act as physical stimuli to assist in hydrogel formation.[34,35] No significant solubility was achieved in water, pH 5.5 even after sonication and heating and no gel was formed upon cooling. Interestingly, in case of phosphate buffer solution (PB) at pH 7.4, the FmocF at 6 mg/mL concentration (0.6% w/v) first gave milky appearance after sonication and dissolved successfully on heating. A transparent gel was formed on cooling at room temperature within few minutes as shown in schematic (Fig. 2). The gel does not flow on the vial inversion and showed fibrous nature when observed under optical microscope (Fig. S1 and S2†). Interestingly, only heating or sonication alone did not result in gel formation at 6 mg/mL concentration. Further, we have not observed any significant change in particle size before and after sonication of FmocF solution (Fig. S3 and S4†). Size obtained was in micrometre range and at the maximum limit of detection of a DLS instrument. Microscopic analysis also revealed particles as large as 50 μM. Interestingly, there was a significant decrease in polydispersity index (PDI), indicating formation of homogenous solution after sonication (Fig. S3†), which also looks evident from visual inspection (Fig. S5†). Additionally, we have also confirmed the changes in molecular signature by FTIR and found no difference in spectra before and after ultrasonication (Fig. S6†). Only increase in intensity was observed, which further suggests the conversion of FmocF particles to a homogenous suspension.

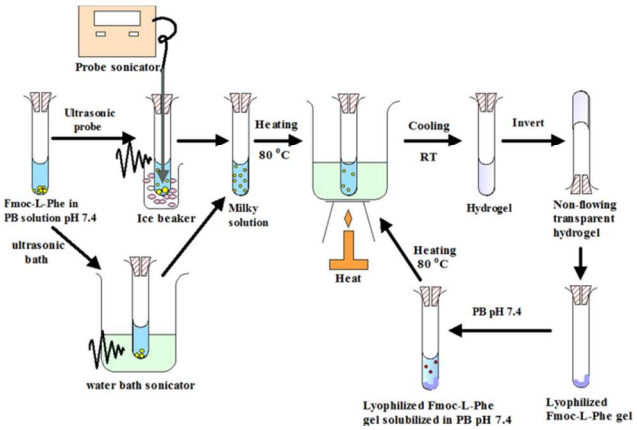

Fig. 2 A schematic of steps involved in FmocF hydrogel formation.

Critical gelator concentration (CGC) of FmocF

CGC is the minimum concentration of a hydrogelator molecule at which the intermolecular interactions start forming leading to the trapping of water molecules to initiate hydrogel formation.[36,37] Above this concentration, gel formation is spontaneous with or without any external perturbation. To calculate the CGC of FmocF, we have used three independent methods.

CGC based on pyrene fluorescence

We have employed pyrene fluorescent probe to determine the CGC of FmocF hydrogel formation. When excited at ~330 nm, pyrene shows two characteristic emission peaks, 380 nm (peak I) and 400 nm (peak III) (Fig. 3a). These peaks are sensitive to the local environment of pyrene and slight variations in it are effectively reflected by the change of emission intensity of these peaks.[38-40] The ratio of peak I/III foretells the polarity and hydrophobicity of the surrounding environment around pyrene.[38-40] To determine CGC, different concentrations of FmocF sample containing pyrene was excited at 334 nm and the emission spectrum was recorded. The CGC was determined by plotting the ratio of peak I and III with respect to the FmocF concentrations (Fig. 3c). The graph shows a sigmoidal decrease of pyrene fluorescence ratio reaching roughly to a constant value. Initially, when FmocF concentration is low, ratio is high indicating presence of pyrene in the more polar environment. With increase in concentration, there is a sharp exponential

decrease in the peak ratio, indicating change in microenvironment of pyrene from polar to non-polar due to efficient packing of FmocF molecules to form hydrogel. Beyond certain limit, there is no comparable change in peak ratio as pyrene remains buried in the hydrophobic regions of fully formed hydrogel.[41]

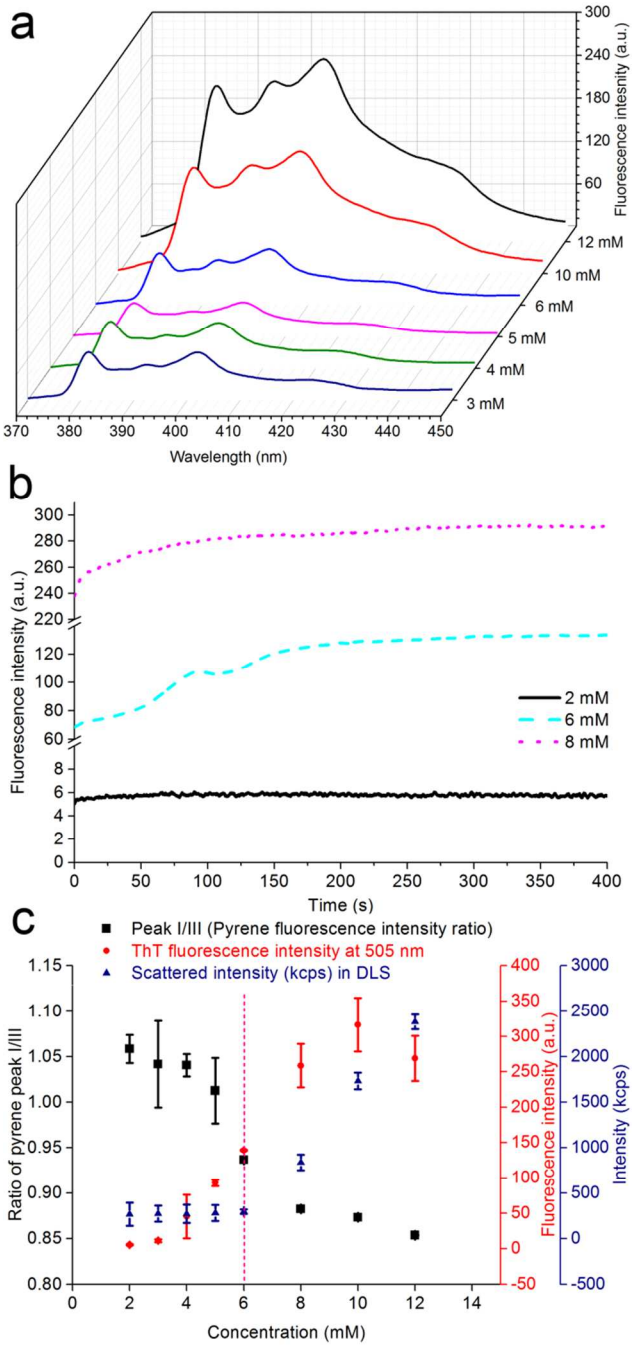

Fig. 3 (a) Pyrene fluorescence emission spectra recorded for different concentrations of FmocF. (b) Thioflavin T fluorescence at different FmocF concentration (c) Fluorescence intensity ratio of pyrene peaks (I/III) as a function of concentration of FmocF. The vertical dotted line represents the estimated value of the critical gelation concentration. Critical concentration determination using the variation of ratio of peaks of fluorescence emission spectroscopy of pyrene, ThT intensity at 505 nm and scattered light intensity (kcps) in DLS with concentration of FmocF.

CGC based on thioflavin T (ThT) fluorescence and dynamic light scattering (DLS)

Thioflavin T is used for detection of amyloid fibres and also to study gel formation, due to its environment dependent emission fluorescence behaviour.[42] Change in fluorescence with time provides a better insight into gel formation kinetics as self-assembly of molecules create more hydrophobic environment for ThT. Same amount of ThT was added to sonicated and heated FmocF samples at different concentrations and allowed to form gel in the cuvette. Real time monitoring of the ThT intensity at an emission wavelength of 505 nm was carried out. At 6 mM FmocF concentration, increase in fluorescence was observed till 200 seconds, which latter stabilized indicating completion of the gel formation (Fig. 3b). Visual observation also confirmed the gel formation within this duration. For 8 mM concentration, there was an initial surge in the fluorescence intensity which latter stabilizes to a constant value. This can be explained by the rapid gel formation with the increase in concentration. For comparison of gel formation at different initial concentrations, fluorescence intensity obtained at each concentration after 20 minutes of starting reaction was plotted. Typical sigmoidal curve was observed, showing increase in intensity with increasing concentration (Fig. 3c).

Similarly, scattered intensity (kcps) was determined using DLS as a function of FmocF concentration (Fig. 3c). The scattered light intensity below 6 mM did not show any increase. But later it increased linearly with increasing concentration. This is probably due to start of formation of higher order assemblies, an initial step in the FmocF ~~self-association~~self-association toward gel formation. Below this concentration enough molecules are not available to self-assemble. Similar behaviour was earlier reported for PB-b-PEO copolymer in which CMC was determined based on abrupt change in intensity (kcps) beyond certain concentration using DLS.[41]

Combination of these three techniques was used to calculate CGC of FmocF hydrogel formation (Fig. 3c). The intersection of the data points obtained from three techniques corresponds to ~6 mM. This suggests that below this concentration gel formation cannot happen. Therefore, it can be considered as CGC value of FmocF hydrogel formation. Good correlation obtained between three different biophysical methods further validates the data obtained. This establishes that any of these techniques can be used for the determination of CGC for hydrogel systems.

Factors governing FmocF gelation

Gel formation is not only the property of a molecule but, solution conditions play equal role in facilitating gel formation. We have tested some of these factors contributing towards gel formation of FmocF.

Effect of pH and buffer

Having established the hydrogel formation in phosphate buffer, we tested the effect of pH on hydrogel formation within buffering range of phosphate buffer (pH 5.8 to 8.0).

Surprisingly, no gel was formed at pH 5.8, 6.0 and 6.5 (Fig. 4). The Gel was formed at pH 7.0, however it required a longer duration of heating (30 minutes) to solubilize. Gel was also obtained at pH 7.5 and 8.0 as shown in figure 3. The pKa of FmocF is predicted to be about 3.5.[43] So, ideally it carries a negative charge at pH 7.4, where it forms gel. It can be postulated that negative charge may cause electrostatic repulsion and inhibits self-assembly. But as reported in the case of FmocFF, there is an apparent increase in pKa of this molecule due to more hydrophobic nature, which puts the charged carboxylate group into hydrophobic environment.[37,43,44] Similarly, it might result in more neutral species of FmocF at pH 7 than anionic ones. Also, assembly formation at pH 7 hints towards the major contribution from hydrophobic interactions, which takes over electrostatic repulsive forces to form gel.

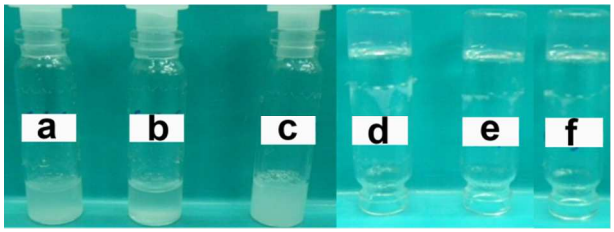

Fig. 4 FmocF (15.5 mM) in phosphate buffer at pH (a) 5.8 (b) 6.0 (c) 6.5 (d) 7.0 (e) 7.5 (f) 8.0. Formation of gel is shown by vial inversion.

Further, we have tested potassium phosphate buffer at pH 7.4, instead of sodium phosphate buffer. Hydrogel was obtained irrespective of sodium or potassium ions used in the buffer. Then to identify the buffer specific behaviour, 50 mM Tris buffer (pH 7.4) was used. Surprisingly, FmocF at 6 mg/mL concentration did not dissolve completely and no gel was obtained after heating and sonication. This highlights the importance of pH and buffer constituents in gel formation. Based on our observations, we speculate two possibilities. One could be the assistance provided by the ions in enhancing solubility of FmocF molecule to form super saturated solution and the second could be the involvement of buffer ions in cation-pi/anion-pi interactions between the buffer and FmocF molecules.[45-49]

Gelation behaviour of FmocF in phosphate buffer was further probed using solvent switch strategy, wherein FmocF was dissolved in organic solvent followed by titration with aqueous solution.[50] FmocF solution in DMSO (6 mg/mL) was slowly titrated with different buffers to final 10% (v/v) DMSO concentration. To dissolve FmocF in DMSO, only vortexing is enough with no requirement of sonication or heating. We have tested water pH 5.5 and pH 7.4, Tris pH 7.4, phosphate buffer pH 7.4 and HEPES buffer pH 7.4. Upon titration with phosphate buffer at pH 7.4, Fmoc solution in DMSO turned milky and then become clear after vortexing. Upon overnight incubation at room temperature, solution transformed to hydrogel, similar to the one formed by sonication-heating-cooling method. Fascinatingly, no gel was formed in case of Tris pH 7.4 and water (pH 5.5, 7.4) (Table S1†). Solution remained turbid and the particles did not dissolve even after sonication and heating. However, to our surprise, transparent gel was obtained in HEPES/DMSO buffer system. The differential behaviour for gel formation could be due to the presence of more cations in Tris buffer as compared to HEPES and PB at pH 7.4.[51] Recent report highlights dihydrogen phosphate anion ($H_2PO_4^-$) induced reassembly of anthracene containing fluorescence probe.[52] Our results also indicate involvement of anions in hydrogel formation but, need further investigation to find the complete mechanism. Similar results were obtained when 15% DMSO was used.

To investigate the peculiarity of the gel formation in PB and HEPES buffer, we carried out RP-HPLC analysis to look for retention time (RT) shift which can be caused by the loss of chemical integrity of FmocF in different buffer conditions. We found that there was no change in RT irrespective of gel formation by FmocF (Fig. S7†). This signifies the role of non-covalent interactions in the gel formation and not any chemical modification of FmocF. Further to probe into the structural features of FmocF in different buffer conditions, we have carried out BioATR-FTIR spectroscopy. Interestingly, we observed that FmocF spectra in phosphate and HEPES buffer were similar but, different from the one obtained in water (pH 5.5 and 7.4) and Tris 7.4 (Fig. 5).

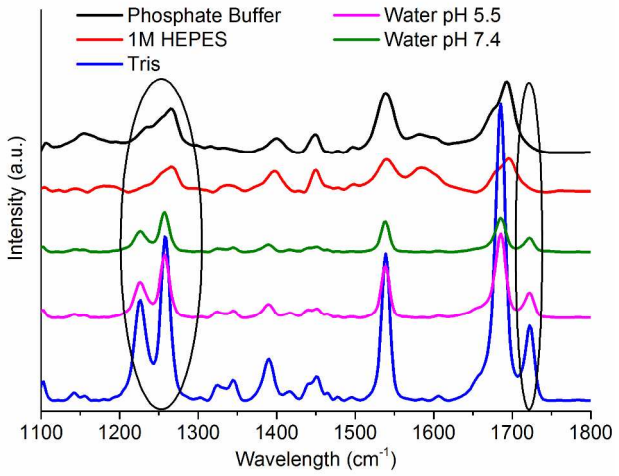

Fig. 5 FTIR spectra of FmocF samples in the presence of 10% DMSO and different buffers. Elliptical circles highlight major spectral differences.

This spectral difference corroborates well for the gel forming condition verses non-gel forming condition. This indicates that non-covalent interactions, an essential feature for gel formation are favourable in phosphate buffer and HEPES buffer. Band at 1720 cm^{-1} in water and Tris buffer diminishes in HEPES and phosphate buffer. This band corresponds to non-hydrogen bonded carbonyl carbamate of Fmoc group,[53] and suggests the involvement of it in hydrogen bonding interaction leading to self-assembly and gelation.[54] Another change was observed in the band between 1200-1300 cm^{-1} which might be due to C-O or C-N stretching. The changes in these bands indicate the molecular reorientation and hydrogen bond formation which with the help of other interaction participate in gel formation.

Molecular contributors of FmocF in driving gel formation

To further analyse the role of molecular contributors within FmocF in the gel formation, we experimented with slightly modified compounds of phenylalanine (Fig. 1a). First we wanted to understand the role played by methylene group of Phe side chain by comparing FmocF with Fmoc-phenylglycine (Fig. S8 and S9†). Notably, no hydrogel was formed by Fmoc-phenylglycine under similar conditions. This elucidates the role of phenylalanine ring with methylene side chain in stacking process and formation of higher order assemblies. It seems that lack of methylene group reduces the flexibility of side chain and hinders the stacking of phenylglycine to gel formation (Fig. 1b). This illustrates the importance of molecular orientation as a necessary factor for FmocF self-assembly to hydrogel transition. Similar effect was reported earlier, where phenylalanine self-assembled to form fibres but phenylglycine failed to self-assemble.[32]

To identify the role of Fmoc, we have tested gel formation by tert-butyloxycarbonyl-L-phenylalanine (BocF) under similar conditions. BocF did not transform to gel, implying the role of Fmoc as the key player in driving the gel formation. This study also proves previous assumptions made by Ulijn and co-authors on Fmoc based peptide hydrogels that Fmoc is the key player in self-assembly process.[20] Unlike Fmoc, Boc is non-aromatic and no gel formation by BocF further suggests the importance of aromatic rings of Fmoc, aiding in the self-assembly to form higher order structures.[20,55] Simultaneously, we have also confirmed that when Fmoc-Cl was mixed with phenylalanine, the mixture did not form the gel. This suggests that covalent linkage between Fmoc and phe is highly important to provide right configuration and interactions for gel formation. To prove whether the gel formation property was specific to FmocF under phosphate buffer conditions, other Fmoc amino acid derivatives were tested. Surprisingly, except tyrosine and methionine derivatives, none others transformed to gel state (Table S2†). These results need further experimentation for mechanistic understanding.

Stereoisomerism and hydrogel formation

Over the years, many research groups have established anti-microbial potential of D-amino acids.[56-58] Also, it was reported that presence of Fmoc moiety further augment anti-microbial action.[59] Considering potential antimicrobial application, we tested capability of Fmoc–D-phenylalanine (Fmoc-D-Phe) for hydrogel formation. Under similar conditions, we found that the Fmoc-D-Phe formed hydrogel, suggesting that hydrogel formation is not specific to D or L configuration (Fig. S10†). We further checked the behaviour of racemic mixture of Fmoc-L-Phe and Fmoc-D-Phe. Interestingly, racemic mixture also formed hydrogel (Fig S10c†). This is in contrast to the behaviour of phenylalanine alone, where DL-phenylalanine formed flakes as compared to fibres formed by L-Phe and D-Phe.[32] Hydrogel formation by Fmoc-D-Phe makes it suitable for biological applications where slow matrix degradation is desired with additional anti-microbial activity.

Our results show that the FmocF hydrogel formation is not dependent on one factor but multiple factors dictate the formation of the hydrogel. Based on the overall experimental observations, we found four necessary components (a) Fmoc as a hydrophobic gelator (b) phenylalanine hydrophobic side chain and its flexibility (Fig. 1b) (c) pH and (d) buffer supporting ionic interactions. These findings further motivated us to characterize the process of hydrogelation and seek for the intervening forces.

Characterization of FmocF hydrogel

^{1}H NMR analysis

To characterize the solution behaviour to gel formation, 1D proton NMR spectra of FmocF was obtained. We have observed upfield shift of aromatic ring protons of Fmoc (>7.2 ppm) group and phenyl ring protons (7-7.2 ppm).[60] With increasing concentration, peak broadening was observed with complete loss of spectral features at 6 mg/mL where solution transforms to gel state (Fig. 6).

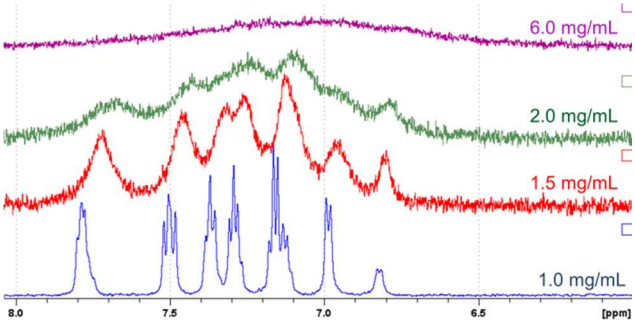

Fig. 6 ^{1}H NMR of FmocF in deuterated phosphate buffer at concentrations ranging from 1 mg/mL to 6 mg/mL.

Upfield chemical shift for aryl protons indicates the involvement of hydrophobic rings in stacking interactions, leading to the gel formation.[19,32,61] Complete loss of spectral features were observed at higher concentration, indicating the complete shift of the environment of protons in solution phase to gel phase.[19]

Nuclear Overhauser NMR spectroscopy (NOESY)

With little insight gained on self-assembly of FmocF in aqueous solution from 1D ^{1}H NMR experiment, we further investigated the role of aryl protons from Fmoc and phenylalanine for their close proximity, while forming hydrogel. Two dimensional NOESY experiment of FmocF was carried out in liquid non gelated state (20% DMSO-d6) and at transition state from liquid to hydrogel (17% DMSO-d6).[62] Solvent switch method was used for NMR spectra recording, as it was difficult to get enough time to record quality spectra in only buffer aqueous solution due to quick gelation. In the presence of 20% DMSO-d6, only two expected short range off-diagonal cross peaks between hydrogen atoms of methylene groups were present (Fig. 7a). Absence of other off-diagonal cross peaks confirmed that other protons are not close enough

to provide interactions through space, indicating solution phase of FmocF.

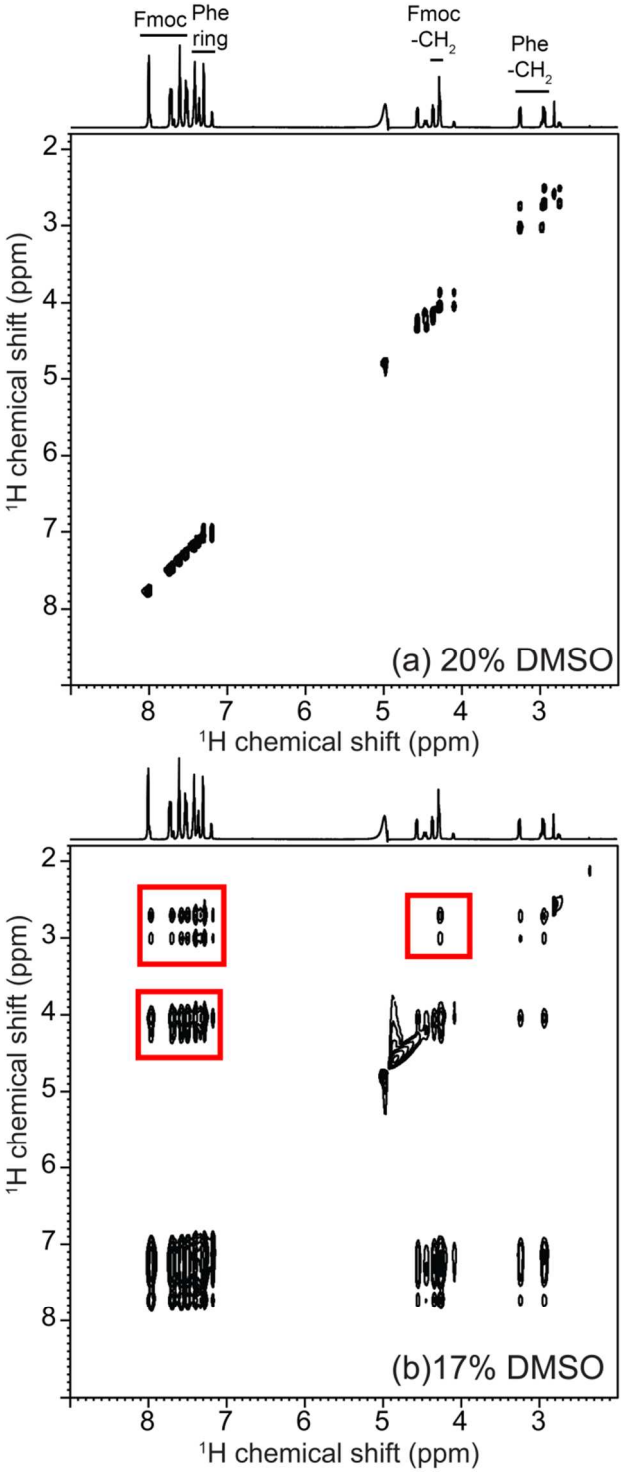

Fig 7 2D NOESY ^{1}H spectra of FmocF (0.6% w/v) in DMSO-d6 (a) 20% DMSO-d6 with 80% deuterated phosphate buffer (pD 7.4) (b) 17% DMSO-d6 with 83% deuterated phosphate buffer (pD 7.4). The off-diagonal cross peaks are highlighted with square.

Interestingly, in gel forming 17% DMSO-d6, off-diagonal cross peaks were observed between the methylene hydrogens of phenylalanine side chain and methylene of Fmoc linker region (Fig. 7b). We also observed off-diagonal cross peaks between aromatic ring and methylene group protons of both Fmoc and phenylalanine. Also, cross peaks were observed for Fmoc and Phe aromatic protons. The presence of cross peaks authenticates the role of intermolecular interactions in the hydrogel formation. The characteristic NOEs obtained in 2D NOESY experiment confirms that Fmoc and phenylalanine rings are interacting with each other in space through hydrophobic interactions. Interestingly, this also brings methylene group of Fmoc and phenylalanine in close proximity, within the range of hydrophobic interactions.

Powder X-ray diffraction

Powder diffraction provides information about the atomic arrangement and microstructure of a molecule and helps to differentiate between crystalline, semicrystalline and amorphous materials. Diffraction pattern for lyophilized FmocF gel and FmocF powder was obtained. The powder form showed sharp distinct peaks and therefore crystalline in nature, whereas lyophilized gel showed broad peaks representing semicrystalline characteristics.[63] This represents that FmocF can be present in two different polymorphic states (Fig. 8a). This also suggests that FmocF after transition to hydrogel might exist as hydrated form providing semicrystalline nature to it. Similar polymorphic states were earlier reported for other small molecules such as phenylalanine.[64-66] After processing XRD data, we have observed characteristic peaks with d-spacing of 11.7 Å as inter-sheet distance, 4.8-4.9 Å corresponds to inter-strand distance and 3.4 Å representing π-π stacking between aromatic rings (Fig. 8b).[17,30,67-69]

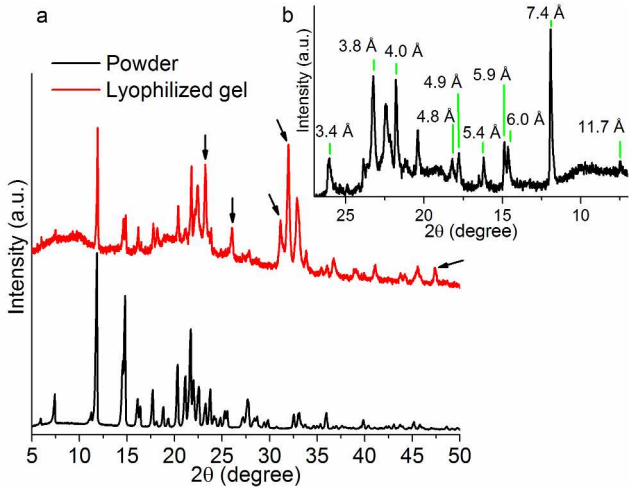

Fig. 8 (a) Powder X-ray diffraction (PXRD) of FmocF powder and lyophilized gel. (b) d-spacing of FmocF lyophilized gel.

FTIR study of polymorphic forms

To further confirm the existence of polymorphic forms, we have compared infrared spectra of FmocF powder and lyophilized FmocF. Notably, band at 1720 cm^{-1} which corresponds to carbonyl carbamate of Fmoc group was diminished in lyophilized gel spectra (Fig. 9).[54] Fascinatingly this feature retained from the gel state to the lyophilized gel.

This might be either due to involvement of this carbonyl in hydrogen bonding or different environment caused by Fmoc group upon interaction. Difference in two spectra confirmed the presence of new polymorphic form of FmocF. We have also compared band intensity at 1254 cm^{-1} and 894 cm^{-1}. The band at 1536 cm^{-1}, representing amide NH bending, was considered as reference band,[70,71] as there is no change in intensity for this peak (Fig. S11†). In lyophilized gel, –CH bending out of plane (oop) band at 894 cm^{-1} was diminished whereas the intensity of C-O or C-N stretch band at 1254 cm^{-1} was decreased by 40% (Fig. S11†). No change in retention time was observed for both samples in RP-HPLC, indicating absence of any chemical modification (Fig. S12†). Also, there was no comparable change in FTIR spectra of FmocF gel and lyophilized gel, indicating retention of molecular arrangement signature after lyophilization (Fig. 5 and 9). It confirms the persistence of different polymorphic state even after lyophilization. Further, to confirm and distinguish between two polymorphs, we have carried out hydrogen deuterium exchange experiment. Interestingly, hydrogen deuterium exchange in case of FmocF powder resulted in no spectral change whereas, lyophilized gel showed different spectra. Bands at 1254 cm^{-1} and 1536 cm^{-1} shifted after deuterium exchange in lyophilized gel, while no such change was observed in FmocF powder (Fig. S13†). This confirms different packing of two FmocF polymorphic states.

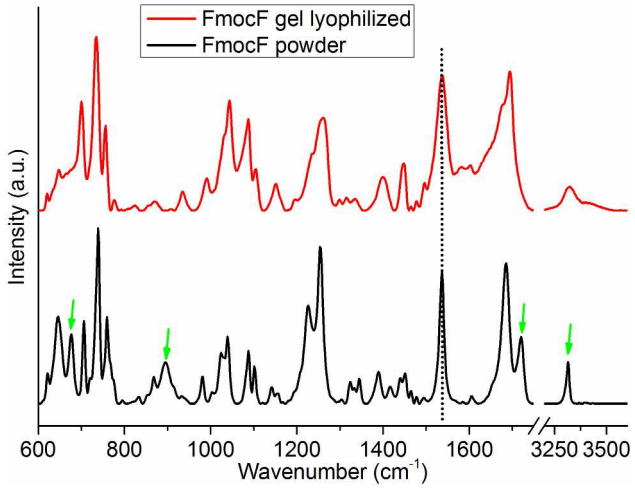

Fig. 9 FTIR spectra of FmocF powder obtained from the supplier and FmocF lyophilized gel. Peak at 1536 cm^{-1} (dotted vertical line) represents reference peak.

Interesting features in the FmocF hydrogel were observed when probed with different biophysical techniques. Though an upfield shift in proton NMR spectra was expected due to involvement of hydrophobic interactions, the presence of off-diagonal cross peaks in 2D NOESY proton NMR spectra highlights the importance of the hydrophobic interactions and arrangement of FmocF molecules. The use of powder XRD and FTIR techniques confirmed the presence of new polymorphic form of FmocF formed after hydrogelation. This highlights the importance of different interactions during phase transition of FmocF from solution to gel state. After studying the intricacies involved in FmocF hydrogel formation and forces controlling the whole process, we probed into the suitability of hydrogel for biomedical application.

Dye release kinetics

Hydrogels are projected in numerous biomedical applications and are currently used for contact lenses and wound care.[72] Fmoc-peptide cationic amphiphiles and mixture of FmocF with Fmoc-leucine were reported to show antimicrobial activity, especially against gram-positive bacteria.[73,74] Earlier reports have suggested the use of FmocF and naphthalene-1-acetamide of L-phenylalanine hydrogel for dye entrapment and release.[37,75,76] However, the dye release kinetics from these hydrogels was not completely understood. Therefore, we thought of using FmocF hydrogel as antimicrobial as well as matrix for controlled drug release. So we probed the release kinetics of model dyes from FmocF hydrogel to give a working model for drug release.

Before setting up the dye release assay, we tested the congo red and direct red dye diffusion through the gel. This was important to establish the presence of water channels within the hydrogel. We have observed diffusion of dyes in both upward and downward direction (Fig. S14†). This experiment established that hydrogel is porous in nature which enables free diffusion of small molecules across gel matrix and dye did not bind specifically to the gel. To study the dye release kinetics, dye was entrapped in the gel by adding dye to FmocF solution and allowed to form gel. Interestingly dye itself did not change the property of gel formation by FmocF. Dye release was monitored by light absorbance and cumulative dye release was plotted against time (Fig. 10a).

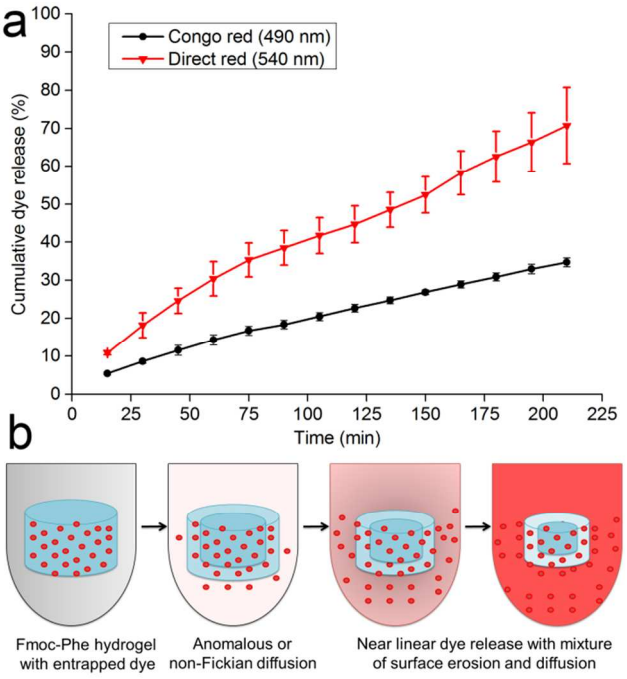

Fig. 10 (a) Cumulative dye release of congo red and direct red with time from the hydrogel (b) Model for dye release from FmocF hydrogel matrix showing anomalous behaviour. Red dots represent dye molecules.

We fit the release data to nonlinear models using SigmaPlot. Among the five models tested, Peppas model gave the best fit with highest goodness of fit (R^2) value. This model fitted well for both the dyes, irrespective of dye molecular weight with coefficient value of about 0.7 (0.43 and 0.85), indicating anomalous or non-Fickian diffusion (Table S3†).[61,62] This indicates near linear dye release with mixture of gel surface erosion and dye diffusion.[77,78] To validate this, we monitored FmocF release from the gel matrix with and without entrapped dye using RP-HPLC method. We have found that with time FmocF was lost from the hydrogel to solution in both cases, indicating surface erosion (Fig. S15†). Based on these observations we are proposing a probable working model of drug release in which dye entrapped in FmocF hydrogel slowly diffuses out. Simultaneously, gel undergoes surface erosion due to loss of FmocF molecules to release more dye into the solution leading to reduction in gel size and increase in color intensity (Fig. 10b and S16†).

To further assess dye release and gel degradation, FmocF and dye release were studied at different temperatures. Temperature range was chosen based on gel stability for atleast 24 hours (Fig. S17†). Vial inversion test was carried out to test gel stability. Further, structural integrity of gel was checked by comparing FTIR spectra at different temperatures (Fig. S18†). Hydrogel spectral features were present at 25 ^{o}C and 45 ^{o}C where it exists in gel state whereas spectral features were lost at 65 ^{o}C where it remains in liquid state. Spectral difference at 1586 cm^{-1} corresponds to deprotonated carboxyl group at 65 ^{o}C, which got involved in ionic interactions at lower temperature. Both FmocF and dye showed enhancement in release with temperature (Fig. 11).

With increase in temperature from 4 ^{o}C to 25 ^{o}C, rate of gel matrix disintegration to release FmocF and dye release due to diffusion and gel surface erosion increased slightly. But beyond 25 ^{o}C, abrupt change in release was observed for both FmocF and dye. This is due to faster gel erosion and enhanced dye diffusion at higher temperature. Also, the percent cumulative release for dye is more comparative to FmocF, which validates our proposed model wherein the drug release is due to diffusion as well as gel surface erosion. Additionally, the hydrogel integrity and stability at higher temperature suggests that the gel can be used at wide range of temperatures making it suitable for biomedical application.

Conclusions

In summary, we have reported the involvement of multiple factors in hydrogel formation of Fmoc-L-phenylalanine in aqueous phosphate buffer. It has been observed that FmocF gelation is not just dependent on pH but, buffer ions play an important role in driving the self-assembly process. Further, we report that the non-covalent ionic interactions and hydrophobic stacking interactions fortify the gelation process. Based on NMR results, we confirmed the important role of phenylalanine side chain, wherein the phenylalanine ring comes in close proximity to Fmoc moiety in space to form stacks of FmocF molecules, leading to gelation. This implicates methylene group in self-assembly of FmocF. We will like to highlight that the above mentioned results hold true for the buffer conditions used and may vary under different buffer and solvent conditions.

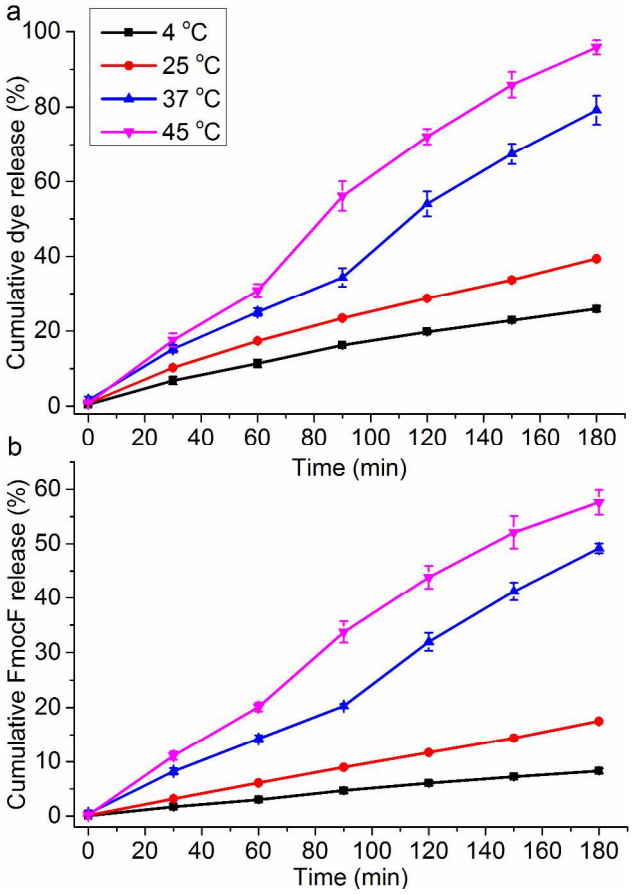

Fig. 11 (a) Cumulative dye release of direct red from the hydrogel with time at different temperatures (b) Cumulative FmocF release from hydrogel matrix with time at different temperatures.

Further, we have reported and characterized a novel polymorphic form of FmocF obtained after transition to hydrogel. The molecular signature of this form is also retained in the lyophilized form. Finally, our study offers a model for drug entrapment and release study and also provides an opportunity to develop into a biodegradable matrix. In addition, Fmoc-D-Phe hydrogel can be tested for additional advantage as an anti-microbial agent. Further with understanding of gel formation and factors involved in driving gelation, new Fmoc derivatives can be designed with better biocompatibility. The mechanistic insights into the self-assembly to gel formation will facilitate the development of tailor made non-covalent hydrogelators that are easier and cheaper to synthesise for a given application.

Experimental

Materials

All Fmoc amino acids (min. 99% pure) were purchased from sisco research laboratory (SRL), Fmoc chloride, L-(+)-α-

phenylglycine, pyrene, congo red, direct red 80 and DMSO from Sigma. Di-sodium hydrogen phosphate, sodium dihydrogen phosphate, Tris, HEPES, methanol, acetonitrile and hydrochloric acid were obtained from Merck and used as received. MilliQ water (18.2 mΩ.cm) was used throughout this study. All chemicals were used as received.

Hydrogel preparation

The FmocF (6.0 mg) was suspended in 1 mL of 50 mM sodium phosphate buffer pH 7.4. The sample was sonicated using Laczene Biosciences bath sonicator at 25 ^{o}C or MSE Soniprep 150 probe sonicator until a homogenous solution was obtained. Sample was gently heated at 80 ºC for 10 minutes to aid dissolution. For formation of hydrogel, the samples were left undisturbed for 24 hours at room temperature (25 ^{o}C). Throughout the whole study hydrogel of all Fmoc amino acid derivatives was prepared by following the above steps in sodium phosphate buffer. FmocF hydrogel was prepared at 6 mg/mL (15.5 mM/0.6% w/v) concentration in phosphate buffer pH 7.4 throughout the study, unless stated otherwise. For mixture of Fmoc-Cl and Phe, 8 mM of each constituent was dissolved in DMSO and titrated with 85% phosphate buffer pH 7.4.

Effect of pH and buffer

To study the effect of pH, 50 mM sodium phosphate buffer of pH 5.8, 6.0, 6.5, 7.0, 7.5 and 8.0 was prepared and 6 mg FmocF was dissolved in it, as described above. The samples were left undisturbed for 24 hours. Formation of gel was identified by the inversion test. Phosphate buffer was prepared using di-sodium hydrogen phosphate (50 mM) and sodium dihydrogen phosphate monohydrate (50 mM). For preparation of potassium phosphate buffer, di-potassium hydrogen phosphate (50 mM) and potassium dihydrogen phosphate monohydrate (50 mM) were used. 50 mM Tris pH 7.4 and 1M HEPES pH 7.4 were used. For solvent switch assay, 6 mg of FmocF (0.6% w/v) was dissolved in 100 µL DMSO using vortex and different buffers were added slowly to make up 1 mL volume. Sample was vortexed until it became clear and left at room temperature overnight for gel formation. Samples were analysed by RP-HPLC at 215 nm wavelength on Agilent HPLC 1260 using ZORBAX Eclipse Plus C18 Rapid Resolution (4.6 × 100 mm, 3.5 µm) column with water and acetonitrile, each containing 0.05% TFA as mobile phase.

Critical gelation concentration (CGC) determination using pyrene fluorescence

Stock solution was prepared by dissolving 1.0 mg pyrene in 2ml of methanol; 5 µl of 20 time's diluted stock was added to 150 µl of FmocF solution prepared at concentrations ranging from 2 mM to 12 mM in phosphate buffer. These samples were excited at 334 nm with excitation and emission slit width of 10 nm and 3 nm, respectively using PerkinElmer LS55 fluorescence Spectrometer. Continuous scanning was performed from 350 nm to 500 nm at 300 nm/min scan speed. The ratio of the intensity of first (380 nm) and third peak (400 nm) was plotted against concentration to determine the CGC. The experiment was performed thrice and the average reading is reported here along with the standard deviation.

Gel kinetics and CGC determination using thioflavin T (ThT) fluorescence

To 200 µl of different concentrations of FmocF solution, 7 µL of 2.5 mM ThT solution was added and immediately transferred into a 1.0 cm path-length cuvette for analysis. Emission spectra were collected from 460 nm to 600 nm in a continuous mode till gel formation by ThT excitation at 450 nm. The emission maxima was at observed at 505 nm. The slit width was set at 3 nm for emission and 5 nm for excitation with 300 nm/min scan speed. The experiment was repeated thrice and average value has been reported.

Dynamic light scattering (DLS)

For determination of CGC, DLS was performed on Malvern Zetasizer Nano ZS90 equipped with He–Ne laser operating at a wavelength of 633 nm and an angle of 90°. Heated sample solutions at concentrations ranging from 2 to 12 mM were filtered through 0.45 µm syringe filter into glass cuvette before analysis. All the DLS measurements were performed at 25 ºC. Particle size (intensity/kcps) was recorded and plotted against concentration.

Fourier transform infrared spectroscopy (FTIR)

A spectrum was collected using Bruker Tensor 27 spectrometer equipped with MCT/DTGS detector and BioATR/ZnSe-ATR accessory. For BioATR FTIR, liquid nitrogen cooled MCT detector was used. We took 20 µL of sample to record spectra. Buffer without FmocF was used for background correction and subtracted from the sample. Spectra were acquired from 4000–850 cm^{-1} at a resolution of 4 cm^{-1} with 120 scans per sample. For samples before and after ultrasonication, 30 µL of sample was used. For ATR FTIR, vacuum dried samples were pressed onto the crystal using the attached high-pressure clamp equipped tip. The air spectrum was used as background and subtracted from all spectra. Spectra were acquired from 4000–600 cm^{-1} at a resolution of 4 cm^{-1} with 120 scans per sample. All spectra were corrected for atmospheric CO_2 and water prior to baseline correction using rubberband method with 64 iterations. Hydrogen deuterium exchange was carried out by mixing FmocF powder and lyophilized gel in deuterium oxide. Samples were vortexed and incubated for 4 h at room temperature and were dried in a vacuum desiccator for 12 h. Process was repeated twice for maximum deuterium exchange before analysis.

Proton nuclear magnetic resonance (^{1}H NMR)

^{1}H NMR spectra were recorded on JEOL ECX-500 instrument (500 MHz). FmocF samples at concentrations ranging from 1 mg/mL to 6 mg/mL were prepared in deuterated sodium

phosphate buffer. Data was recorded at room temperature and processed using Bruker TopSpin v3.2 software.

2D NOESY NMR

500 µL FmocF sample was prepared by dissolving 3 mg of sample in DMSO-d6 and then titrated with deuterated phosphate buffer pD 7.4 slowly and vortexed till clear solution was obtained. Sample with 20% DMSO-d6 and 17% DMSO-d6 were used for analysis. 2D NOESY spectra were recorded with solvent pre-saturation on Bruker 800-MHz NMR spectrometer equipped with a triple-resonance TCI (^{1}H, ^{13}C, ^{15}N, and ^{2}H lock) cryogenic probe. D_2O inside the buffer was used for lock. 8 transients were recorded with relaxation delay of 2 s, 900 pulse lengths of 7.91 µs, 256 t1 points and 300 ms mixing time. The data was processed using Bruker Topspin 2.1 software with 0.3 Hz of line broadening. Phase correction was performed in both dimensions (t1 and t2).

Powder X-ray diffraction (PXRD)

FmocF powder and lyophilized FmocF hydrogel were loaded into a trough of glass sample holder and smoothing of surface was done with glass slide. Powder diffraction analyses was carried out on PANalytical X'Pert Powder diffractometer with CuKα (λ = 1.54 Å) radiation. Samples were scanned over range of 4º to 50º 2θ with step size was 0.0131 degrees. The d-spacing was calculated using $d = \lambda/(2 \sin\theta)$ where λ (Cu kα) is fix 1.54 Å, θ in radians.

Dye release

Stock solutions (1 mg/mL) of congo red (CR, Mol. Wt. 696 Da) and direct red 80 (DR, Mol. Wt. 1371 Da) dyes were prepared in phosphate buffer pH 7.4. For upward diffusion of dyes through the gel matrix, preformed gel was placed on top of 10 µL of dye. It was kept overnight at room temperature. Similarly, 10 µL of dye was added on the top of the preformed gel and left undisturbed for overnight at room temperature. For dye release kinetics, 15 µL (15 µg) of dye was added to 185 µL of 6 mg/mL heated FmocF solution. Solution was allowed to cool at room temperature to form gel with entrapped dye. Dye release was carried out by addition of 200 µL phosphate buffer pH 7.4 and incubated at 37 ^{o}C without stirring. Sampling was done at regular intervals of 15 minutes by aspirating 200 µL of buffer and replacing it with equal volume of fresh buffer to maintain constant volume. Absorbance of sample collected in 96 well microplate was measured at 490 nm for CR and 540 nm for DR using spectraMax M3 instrument. Maximum dye entrapped was determined by taking absorbance of 1 mg/mL dye dissolved in PB pH 7.4 and used to calculate percentage cumulative dye release. Average of triplicates with standard deviation was plotted against time. The data was fit with nonlinear models for the controlled release of pharmaceuticals using SigmaPlot version 12.0, from Systat Software, Inc., San Jose California USA, www.sigmaplot.com). Gel degradation was monitored by RP-HPLC method as described earlier. Sample was analysed every 30 min for 2 hours. For temperature dependent release study, experiment was carried out using above mentioned procedure. To minimize errors, buffer was also maintained at respective temperature. Simultaneously, the dye release was monitored by absorbance at 540 nm and FmocF release by RP-HPLC. Average of triplicates with standard deviation was plotted against time.

Statistical analysis

Results are presented as mean±SD unless stated otherwise. Comparisons between any two groups were performed using two-tailed unpaired Student's t-test. Differences were considered statistically significant when $P < 0.05$.

Acknowledgements

Virender Singh and Chandan Singh gratefully acknowledge financial support from the Council of Scientific and Industrial Research (CSIR), India. Chandan Singh and Neeraj Sinha helped in recording 2D NOESY NMR spectra and data interpretation. This work was supported by a grant from the Department of Biotechnology (DBT), Government of India grant no. BT/PR3041/NNT/28/545/2011 and IIT Kanpur research initiating grant IITK/BSBE/20100226. We thank Professor S. Ganesh, BSBE, IIT Kanpur for providing the microplate reader facility and Anupama Rai for assistance in handling the instrument. We also thank Dr. Saravanan Matheshwaran for providing ultrasonicator and Ashta Gupta for helping in ESI MS of Fmoc-phenylglycine.

Footnotes

‡ These authors contributed equally.

[a]Department of Biological Sciences and Bioengineering, Indian Institute of Technology Kanpur, Kanpur, Uttar Pradesh, 208016, India, email: akthakur@iitk.ac.in; Fax: +91-512-259-4010; Tel: +91-512-259-4077.

[b]Department of Biology, University of Dayton, Dayton, USA.

[c]School of Biotechnology, Faculty of Science, Banaras Hindu University, Varanasi, 221005, India

[d]Centre of Biomedical Research, Sanjay Gandhi Postgraduate Institute of Medical Sciences Campus, Lucknow, 226014, India

†Electronic Supplementary Information (ESI) available. See DOI: 10.1039/

§Structure drawn using ACD/Chemsketch, Version 14.01 and release 2012.

References

1. K. E. Routledge, G. G. Tartaglia, G. W. Platt, M. Vendruscolo and S. E. Radford, *J. Mol. Biol.*, 2009, **389**, 776-786.
2. Y. Tang, C. L. Heaysman, S. Willis and A. L. Lewis, *Expert Opin. Drug Deliv.*, 2011, **8**, 1141-1159.
3. P. Duan, H. Cao, L. Zhang and M. Liu, *Soft Matter*, 2014, **10**, 5428-5448.
4. A. Pasc, F. Obounou Akong, S. Cosgun and C. Gerardin, *Beilstein J. Org. Chem.*, 2010, **6**, 973-977.

5. M. Nishio, Y. Umezawa, J. Fantini, M. S. Weiss and P. Chakrabarti, *Phys. Chem. Chem. Phys.*, 2014, **16**, 12648-12683.
6. A. K. Gaharwar, N. A. Peppas and A. Khademhosseini, *Biotechnol. Bioeng.*, 2014, **111**, 441-453.
7. A. N. Rissanou, E. Georgilis, E. Kasotakis, A. Mitraki and V. Harmandaris, *J. Phys. Chem. B*, 2013, **117**, 3962-3975.
8. C. Guo, Y. Luo, R. Zhou and G. Wei, *ACS Nano*, 2012, **6**, 3907-3918.
9. C. Guo, Y. Luo, R. Zhou and G. Wei, *Nanoscale*, 2014, **6**, 2800-2811.
10. Z. Luo, S. Wang and S. Zhang, *Biomaterials*, 2011, **32**, 2013-2020.
11. H. Yokoi, T. Kinoshita and S. Zhang, *Proc. Natl. Acad. Sci. U. S. A.*, 2005, **102**, 8414-8419.
12. H. Cui, M. J. Webber and S. I. Stupp, *Biopolymers*, 2010, **94**, 1-18.
13. S. Koutsopoulos, L. D. Unsworth, Y. Nagai and S. Zhang, *Proc. Natl. Acad. Sci. U. S. A.*, 2009, **106**, 4623-4628.
14. A. S. Hoffman, *Adv. Drug Deliver. Rev.*, 2012, **64**, 18-23.
15. D. J. Adams and P. D. Topham, *Soft Matter*, 2010, **6**, 3707.
16. Y. Zhang, Y. Kuang, Y. Gao and B. Xu, *Langmuir*, 2011, **27**, 529-537.
17. S. Fleming and R. V. Ulijn, *Chem. Soc. Rev.*, 2014, **43**, 8150-8177.
18. G. Fichman and E. Gazit, *Acta Biomater.*, 2014, **10**, 1671-1682.
19. D. M. Ryan, T. M. Doran, S. B. Anderson and B. L. Nilsson, *Langmuir*, 2011, **27**, 4029-4039.
20. S. Fleming, S. Debnath, P. W. Frederix, T. Tuttle and R. V. Ulijn, *Chem. Commun.*, 2013, **49**, 10587-10589.
21. K. M. Eckes, X. Mu, M. A. Ruehle, P. Ren and L. J. Suggs, *Langmuir*, 2014, **30**, 5287-5296.
22. R. Li, C. C. Horgan, B. Long, A. L. Rodriguez, L. Mather, C. J. Barrow, D. R. Nisbet and R. J. Williams, *RSC Adv.*, 2015, **5**, 301-307.
23. J. Raeburn, A. Zamith Cardoso and D. J. Adams, *Chem. Soc. Rev.*, 2013, **42**, 5143-5156.
24. A. Mahler, M. Reches, M. Rechter, S. Cohen and E. Gazit, *Adv. Mater.*, 2006, **18**, 1365-1370.
25. R. Vegners, I. Shestakova, I. Kalvinsh, R. M. Ezzell and P. A. Janmey, *J. Pept. Sci.*, 1995, **1**, 371-378.
26. A. M. Smith, R. J. Williams, C. Tang, P. Coppo, R. F. Collins, M. L. Turner, A. Saiani and R. V. Ulijn, *Adv. Mater.*, 2008, **20**, 37-41.
27. M. Zhou, A. M. Smith, A. K. Das, N. W. Hodson, R. F. Collins, R. V. Ulijn and J. E. Gough, *Biomaterials*, 2009, **30**, 2523-2530.
28. V. Jayawarna, M. Ali, T. A. Jowitt, A. F. Miller, A. Saiani, J. E. Gough and R. V. Ulijn, *Adv. Mater.*, 2006, **18**, 611-614.
29. S. Roy and A. Banerjee, *Soft Matter*, 2011, **7**, 5300.
30. A. Saha, S. Bolisetty, S. Handschin and R. Mezzenga, *Soft Matter*, 2013, **9**, 10239-10242.
31. A. J. Patil, R. K. Kumar, N. J. Barron and S. Mann, *Chem. Commun.*, 2012, **48**, 7934-7936.
32. V. Singh, R. K. Rai, A. Arora, N. Sinha and A. K. Thakur, *Sci. Rep.*, 2014, **4**, 3875.
33. J. M. Poolman, J. Boekhoven, A. Besselink, A. G. L. Olive, J. H. van Esch and R. Eelkema, *Nat. Protoc.*, 2014, **9**, 977-988.
34. X. Yu, L. Chen, M. Zhang and T. Yi, *Chem. Soc. Rev.*, 2014, **43**, 5346-5371.
35. C. G. Pappas, T. Mutasa, P. W. J. M. Frederix, S. Fleming, S. Bai, S. Debnath, S. M. Kelly, A. Gachagan and R. V. Ulijn, *Materials Horizons*, 2015.
36. D. Yu, F. Huang and H. Xu, *Anal. Methods*, 2012, **4**, 47.
37. A. Reddy, A. Sharma and A. Srivastava, *Chemistry*, 2012, **18**, 7575-7581.
38. M. Yan, B. Li and X. Zhao, *Food Chem.*, 2010, **122**, 1333-1337.
39. V. Castelletto, G. Cheng, B. W. Greenland, I. W. Hamley and P. J. Harris, *Langmuir*, 2011, **27**, 2980-2988.
40. S. Thirunavukkuarasu, E. A. Jares-Erijman and T. M. Jovin, *J. Mol. Biol.*, 2008, **378**, 1064-1073.
41. O. Topel, B. A. Cakır, L. Budama and N. Hoda, *J. Mol. Liq.*, 2013, **177**, 40-43.
42. S. Grigoriou, E. K. Johnson, L. Chen, D. J. Adams, T. D. James and P. J. Cameron, *Soft Matter*, 2012, **8**, 6788.
43. E. K. Johnson, D. J. Adams and P. J. Cameron, *J. Mater. Chem.*, 2011, **21**, 2024.
44. C. Tang, A. M. Smith, R. F. Collins, R. V. Ulijn and A. Saiani, *Langmuir*, 2009, **25**, 9447-9453.
45. A. Robertazzi, F. Krull, E.-W. Knapp and P. Gamez, *CrystEngComm*, 2011, **13**, 3293.
46. S. Roy, N. Javid, P. W. Frederix, D. A. Lamprou, A. J. Urquhart, N. T. Hunt, P. J. Halling and R. V. Ulijn, *Chemistry*, 2012, **18**, 11723-11731.
47. A. S. Mahadevi and G. N. Sastry, *Chem. Rev.*, 2013, **113**, 2100-2138.
48. D. Quinonero, A. Frontera, C. Garau, P. Ballester, A. Costa and P. M. Deya, *Chemphyschem*, 2006, **7**, 2487-2491.
49. J. P. Schwans, F. Sunden, J. K. Lassila, A. Gonzalez, Y. Tsai and D. Herschlag, *Proc. Natl. Acad. Sci. U. S. A.*, 2013, **110**, 11308-11313.
50. J. Raeburn, G. Pont, L. Chen, Y. Cesbron, R. Levy and D. J. Adams, *Soft Matter*, 2012, **8**, 1168-1174.
51. R. H. Wilson, H. J. Evans and R. R. Becker, *J. Biol. Chem.*, 1967, **242**, 3825-3832.
52. W. T. Gong, D. Na, L. Fang, H. Mehdi and G.-l. Ning, *Org. Biomol. Chem.*, 2015, **13**, 1979-1982.
53. C. S. Wong and K. H. Badri, *Mater. Sci. Appl.*, 2012, **3**, 78-86.
54. P. Bairi, B. Roy, P. Routh, K. Sen and A. K. Nandi, *Soft Matter*, 2012, **8**, 7436.
55. H. Shao and J. R. Parquette, *Chem. Commun.*, 2010, **46**, 4285-4287.
56. I. Kolodkin-Gal, S. Cao, L. Chai, T. Bottcher, R. Kolter, J. Clardy and R. Losick, *Cell*, 2012, **149**, 684-692.
57. I. Kolodkin-Gal, D. Romero, S. Cao, J. Clardy, R. Kolter and R. Losick, *Science*, 2010, **328**, 627-629.
58. A. I. Hochbaum, I. Kolodkin-Gal, L. Foulston, R. Kolter, J. Aizenberg and R. Losick, *J. Bacteriol.*, 2011, **193**, 5616-5622.
59. Z. Yu, W. Qin, J. Lin, S. Fang and J. Qiu, *BioMed Res. Int.*, 2015, **2015**, 11.
60. Z. Huang, S. Guan, Y. Wang, G. Shi, L. Cao, Y. Gao, Z. Dong, J. Xu, Q. Luo and J. Liu, *J. Mater. Chem. B*, 2013, **1**, 2297.
61. I. Maity, T. K. Mukherjee and A. K. Das, *New J. Chem.*, 2014, **38**, 376.
62. S. Brahmachari, S. Debnath, S. Dutta and P. K. Das, *Beilstein J. Org. Chem.*, 2010, **6**, 859-868.
63. A. Chauhan and P. Chauhan, *J. Anal. Bioanal. Tech.*, 2014, **5**, 212.

64. P. A. Williams, C. E. Hughes, A. B. M. Buanz, S. Gaisford and K. D. M. Harris, *J. Phys. Chem. C*, 2013, **117**, 12136-12145.
65. F. S. Ihlefeldt, F. B. Pettersen, A. von Bonin, M. Zawadzka and C. H. Gorbitz, *Angew. Chem. Int. Edit.*, 2014, **53**, 13600-13604.
66. C. E. Hughes, A. Williams, V. Keast, V. Charalampopoulos, G. Edwards-Gau and K. D. M. Harris, *Faraday Discuss.*, 2014.
67. X. Mu, K. M. Eckes, M. M. Nguyen, L. J. Suggs and P. Ren, *Biomacromolecules*, 2012, **13**, 3562-3571.
68. M. Hughes, P. W. J. M. Frederix, J. Raeburn, L. S. Birchall, J. Sadownik, F. C. Coomer, I. H. Lin, E. J. Cussen, N. T. Hunt, T. Tuttle, S. J. Webb, D. J. Adams and R. V. Ulijn, *Soft Matter*, 2012, **8**, 5595.
69. D. M. Ryan, S. B. Anderson, F. T. Senguen, R. E. Youngman and B. L. Nilsson, *Soft Matter*, 2010, **6**, 475.
70. B. Adhikari and A. Banerjee, *Chemistry*, 2010, **16**, 13698-13705.
71. W. Nuansing, A. Rebollo, J. M. Mercero, J. Zuniga and A. M. Bittner, *J. Raman Spectrosc.*, 2012, **43**, 1397-1406.
72. E. Calo and V. V. Khutoryanskiy, *Eur. Polym. J.*, 2015.
73. S. Debnath, A. Shome, D. Das and P. K. Das, *J. Phys. Chem. B*, 2010, **114**, 4407-4415.
74. I. Irwansyah, Y.-Q. Li, W. Shi, D. Qi, W. R. Leow, M. B. Y. Tang, S. Li and X. Chen, *Adv. Mater.*, 2015, **27**, 648-654.
75. S. Sutton, N. L. Campbell, A. I. Cooper, M. Kirkland, W. J. Frith and D. J. Adams, *Langmuir*, 2009, **25**, 10285-10291.
76. W. J. Frith, A. M. Donald, D. J. Adams and A. Aufderhorst-Roberts, *J. Non-Newton. Fluid*, 2014.
77. Y. Fu and W. J. Kao, *Expert Opin. Drug Deliv.*, 2010, **7**, 429-444.
78. A. S. Joshi and A. K. Thakur, *J. Pept. Sci.*, 2014, **20**, 630-639.

